

Effects of vertical inhomogeneity on snow spectral albedo and its implication for optical remote sensing of snow

Xiaobing Zhou

Department of Earth and Environmental Science, New Mexico Institute of Mining and Technology, Socorro, New Mexico, USA

Shusun Li

Geophysical Institute, University of Alaska Fairbanks, Fairbanks, Alaska, USA

Knut Stamnes

Department of Physics and Engineering Physics, Stevens Institute of Technology, Hoboken, New Jersey, USA

Received 13 June 2003; revised 22 August 2003; accepted 5 September 2003; published 12 December 2003.

[1] The spectral albedo of dry, vertically heterogeneous snow is simulated using a multilayer discrete ordinate method radiative transfer code, with single snow grain–scattering parameters calculated either from Mie theory for small grains or from a geometric optics code for large grains. In the near-infrared wavelengths the snowpack is effectively semi-infinite at a depth of around 5 cm; that is, the reflectance is the same as for a deep snowpack. In the visible wavelengths, however, the snow critical depth is more than 50 cm for coarse-grained snow, but the top 5–10 cm layer is the most important one. Two heterogeneous snowpacks with the same average grain size in the topmost layer but with different vertical distributions of grain sizes can have quite different spectral albedos because of greater penetration by visible than by near-infrared radiation. The spectral albedo computed from the multilayer model agrees better with measured albedo when the vertical variability of grain size and the measured composite grain size rather than the measured single grain size are considered. *INDEX TERMS:* 0933 Exploration Geophysics: Remote sensing; 1827 Hydrology: Glaciology (1863); 1863 Hydrology: Snow and ice (1827); 3359 Meteorology and Atmospheric Dynamics: Radiative processes; 3360 Meteorology and Atmospheric Dynamics: Remote sensing; *KEYWORDS:* spectral albedo, snow and ice, optical remote sensing, inhomogeneity, radiative transfer

Citation: Zhou, X., S. Li, and K. Stamnes, Effects of vertical inhomogeneity on snow spectral albedo and its implication for optical remote sensing of snow, *J. Geophys. Res.*, 108(D23), 4738, doi:10.1029/2003JD003859, 2003.

1. Introduction

[2] It is common for a natural snowpack to be composed of snow layers of different characteristics, each of which is more or less a homogeneous layer [Colbeck, 1991], because it is deposited in a series of relatively uniform snowfall periods during deposition. Subsequent metamorphosis, which is mainly determined by varying weather conditions, gravitational load from the top, and arrangement of ice particles, seems to preserve the homogeneous nature of each snow layer over the lifetime of the snow cover. This stratified structure is ubiquitously observed in snow on sea ice [Sturm *et al.*, 1998; Morris and Jeffries, 2001] and on land [Grenfell *et al.*, 1994; Aoki *et al.*, 2000].

[3] Generally, each homogeneous layer within a stratified seasonal snow cover has its own physical, optical, thermal and mechanical properties due to the initial snow condition and thermal history. For remote sensing of snow, physical and optical properties are the main concerns. In scattering theory, the size of a scatterer is an important parameter in

determining the absorption and scattering of the incident electromagnetic signal. The snow grain size affects the single-scattering albedo and absorption in the visible, near-infrared and microwave regions, and thus it is necessary to estimate grain size in order to retrieve spectral albedo and all-wave albedo from remotely sensed data [Wiscombe and Warren, 1980; Nolin and Dozier, 2000; Painter *et al.*, 2003], and to explain the microwave remote sensing of snow water equivalent [Chang *et al.*, 1981; Armstrong *et al.*, 1993]. In the following study of the interaction of solar radiation with snow, a homogeneous snow layer means a snow layer with uniform effective snow grain size, density and texture. In a natural snow cover, the average snow grain size and density show a remarkable variation from the top layers to the bottom layers [Aoki *et al.*, 2000; Morris and Jeffries, 2001]. Because the optical properties of ice vary with wavelength, this vertical inhomogeneity of the snow physical parameters is expected to affect the interaction of solar radiation with the snow cover, and thus the spectral signals received by both ground-based instruments and space-borne satellite sensors such as the Moderate Resolution Imaging Spectroradiometer (MODIS) aboard the Terra and Aqua satellites. Thus understanding

the effect of the vertical structure of a snowpack on the reflectance of snow is required to correctly interpret the snow albedo measurements [Li *et al.*, 2001].

[4] Efforts to model the snow spectral albedo were comprehensively reviewed by *Wiscombe and Warren* [1980] and *Warren* [1982]. Using a simple analytical model based on the delta-Eddington approximation [Joseph *et al.*, 1976], *Wiscombe and Warren* [1980] studied the dependence of the spectral albedo on snow grain size (or age), liquid water content (through increase of effective snow grain size), solar zenith angle, cloud cover (through change of the effective incidence angle), snow thickness, and snow density. A common difficulty in simulating the spectral reflectance of a natural snowpack using a single homogeneous layer is that a grain size that yields good agreement in the near infrared (NIR) between model and measurements results in poor agreement in the visible, and vice versa. Thus picking the grain size measured at the snow surface to represent a homogeneous snowpack, one finds that the modeled NIR albedo may agree well with measurements of a natural snow cover, while the modeled visible albedo is consistently higher than the measured one [Grenfell and Maykut, 1977; Wiscombe and Warren, 1980; Knap *et al.*, 1999]. The discrepancy in the visible region is often attributed to impurities in the snow (soot, dust) [Warren and Wiscombe, 1980; Knap *et al.*, 1999; Aoki *et al.*, 2000]. However, Antarctic snow is generally considered to be very clean. For instance, Kumai [1976] found that the impurity (clay minerals) concentration at the South Pole was 15 ng g^{-1} . Murozumi *et al.* [1969] found that the impurity (terrestrial dust) at Byrd Station, West Antarctica, was 2 ng g^{-1} . Warren and Clarke [1990] found that near the South Pole the impurity (soot) concentration in the snow far from the station was $0.1\text{--}0.3 \text{ ng g}^{-1}$. Thus impurities are generally neglected in modeling of Antarctic snow reflectance [Grenfell *et al.*, 1994]. Most comparisons of measured spectral albedo with modeling for a pure snowpack indicate that a single homogeneous layer model for a vertically heterogeneous natural snowpack cannot explain the observations. Exceptions occur when the snowpacks' top layer is homogeneous and has a thickness of the semi-infinite depth, as observed sometimes in midlatitude regions [Nolin and Dozier, 2000]. Thus Grenfell *et al.* [1994] introduced a two-layer model: a very thin layer with very fine grain size snow on top of a thick layer of snow with much larger grain size. A two-layer model can be used to fit observations very well, but a multilayered model may be needed for application to a snowpack with vertical inhomogeneity and proper interpretation of the results.

[5] Grenfell *et al.*'s [1994] measurements were carried out at South Pole and Vostok in summer, when the air temperature rarely rises above -20°C . The snow is dry so that snow metamorphism proceeds very slowly. Therefore the snow grain radius at the top of the snowpack is very fine ($20\text{--}100 \mu\text{m}$) and the largest grain radius at lower layers is also relatively small ($0.2\text{--}0.5 \text{ mm}$). The snowpack on sea ice in summer is quite different. The air temperature is around 0°C , liquid water content in the snow can increase from dry at the very top to wet at lower layers and slushy at the bottom due to melting and percolation from the top and flooding from the bottom [Jeffries *et al.*, 1994, 2001]. Snow metamorphism proceeds quickly, resulting in much larger snow grain size in the snowpack over sea ice than the snowpack on the Antarctic

continent. The liquid water in snow will most probably combine with the snow grain as a coated layer and shift the snow absorption wavelength position to a shorter wavelength [Green *et al.*, 2002]. The snow classification adopted here complies with the International Association of Scientific Hydrology (IASH) International Classification for Seasonal Snow on the Ground [Colbeck *et al.*, 1990]. Formation of composite grains as new entities from single grains due to melt-refreeze and recrystallization processes etc., including clustered single crystals (6cl) and melt-freeze polycrystalline particles (6mf) [Colbeck *et al.*, 1990] makes the summer snowpack on sea ice a very special snow cover that has coarse ($1.0\text{--}2.0 \text{ mm}$) or even extremely coarse ($>5 \text{ mm}$) texture. Morris and Jeffries [2001] found that snow composite grains constitute most of the snowpack on sea ice in summer while individual single grains account for only a small portion. Like a single grain, a composite grain has its own short dimension and long dimension.

[6] We focus on the effect of the vertical inhomogeneity of grains on snow reflectance using a multilayer model to compute the spectral albedo of snow, and on comparisons of modeling results with highly resolved spectral albedo measurements (spectral resolution: 3 nm) in the $0.33\text{--}1.06 \mu\text{m}$ spectral region on summer snowpacks on sea ice in the Ross Sea, Antarctica. However, note that the wavelength range of the spectroradiometer used to obtain the spectral albedo measurement is limited and thus does not cover the spectral bands in the shortwave infrared region where snow properties are sensitive to grain size of the top layers of snowpacks.

2. Radiative Transfer Modeling Formulation

[7] Let's denote the vertical coordinate as z , with $z=0$ being the top of the scattering and absorbing medium, so that the direction of z is downward. The polar angle θ is defined as the angle between the inverse direction of the z axis and the light traveling direction. This configuration is shown in Figure 1. The optical depth is $d\tau = \sigma_{\text{ext}}(z)dz$. From Figure 1, we can see that $dL = dz/\cos(\pi - \theta) = -\sec\theta dz$. For optical remote sensing in the solar spectrum, the fundamental distinction between upward ($0 \leq \theta \leq \pi/2$, $0 \leq \mu \leq 1$, $\mu = |\cos\theta|$) and downward directions ($\pi/2 \leq \theta \leq \pi$, $-1 \leq -\mu \leq 0$) is recognized so that the general radiative transfer equations for nonpolarized radiation at wavelength λ in a random medium can be separated into two coupled integrodifferential equations [Thomas and Stamnes, 1999]. At any level of optical thickness, it is convenient to distinguish the direct component of the radiance from the diffuse component, especially for the retrieval of reflectance at the ground surface from remotely sensed data. For the upward radiance, there is no direct component, unless specular reflection is taken into account. However, for the downward azimuthally averaged radiance, there are both direct and diffuse components. The azimuthally averaged diffuse upward and downward radiances satisfy the following equations [Thomas and Stamnes, 1999]:

$$\begin{aligned}
 -\mu \frac{dI_{\lambda,df}^{\uparrow}(\tau, \mu)}{d\tau} &= I_{\lambda,df}^{\uparrow}(\tau, \mu) - \frac{\omega_0}{2} \int_0^1 d\mu' P(\tau; \mu; \mu') I_{\lambda,df}^{\uparrow}(\tau, \mu') \\
 &\quad - \frac{\omega_0}{2} \int_0^1 d\mu' P(\tau; \mu; -\mu') I_{\lambda,df}^{\downarrow}(\tau, \mu') \\
 &\quad - \frac{\omega_0}{4\pi} P(\tau; \mu; -\mu_0) F_{\lambda}^S e^{-\tau/\mu_0}
 \end{aligned} \tag{1a}$$

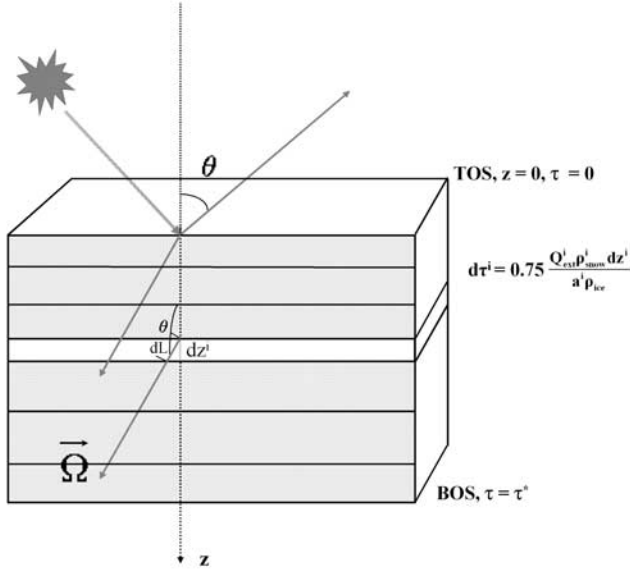


Figure 1. Optical geometry of radiation transport in snowpack. TOS, top of snow; BOS, bottom of snow. See color version of this figure in the HTML.

$$\begin{aligned} \mu \frac{dI_{\lambda,df}^{\downarrow}(\tau, \mu)}{d\tau} &= I_{\lambda,df}^{\downarrow}(\tau, \mu) - \frac{\omega_0}{2} \int_0^1 d\mu' P(\tau; -\mu; \mu') I_{\lambda,df}^{\downarrow}(\tau, \mu') \\ &\quad - \frac{\omega_0}{2} \int_0^1 d\mu' P(\tau; -\mu; -\mu') I_{\lambda,df}^{\downarrow}(\tau, \mu') \\ &\quad - \frac{\omega_0}{4\pi} P(\tau; -\mu; -\mu_0) F_{\lambda}^S e^{-\tau/\mu_0}, \end{aligned} \quad (1b)$$

where

$$\begin{aligned} P(\tau; \mu; \mu') &= \frac{1}{2\pi} \int_0^{2\pi} d(\varphi - \varphi') P(\tau; \mu, \varphi; \mu', \varphi') \\ P(\tau; \mu, \varphi; \mu', \varphi') &= \frac{4\pi C_{sca}^d(\tau, \Theta)}{C_{sca}} = \frac{2C_{sca}^d(\tau, \Theta)}{\int_0^{\pi} d\Theta C_{sca}^d(\tau, \Theta) \sin \Theta} \end{aligned} \quad (2)$$

is the phase function. $C_{sca} = C_{ext} - C_{abs}$ is the total scattering cross section

$$C_{sca} = 2\pi \int_0^{\pi} d\Theta C_{sca}^d(\tau, \Theta) \sin \Theta,$$

and

$$\Theta = \arccos(\mu\mu' + \sqrt{1-\mu^2}\sqrt{1-\mu'^2} \cos(\varphi - \varphi'))$$

is the scattering angle, where φ is the azimuthal angle and θ is the polar angle (see Figure 1). The azimuthally averaged upward radiance at vertical optical depth τ (measured from the snow surface downward to the snow bottom) $I_{\lambda}^{\uparrow}(\tau, \mu)$ and the corresponding azimuthally averaged downward radiance $I_{\lambda}^{\downarrow}(\tau, \mu)$ are determined by

$$I_{\lambda}^{\uparrow}(\tau, \mu) = I_{\lambda,df}^{\uparrow}(\tau, \mu) \quad (3a)$$

$$I_{\lambda}^{\downarrow}(\tau, \mu) = I_{\lambda,dr}^{\downarrow}(\tau, \mu) + I_{\lambda,df}^{\downarrow}(\tau, \mu). \quad (3b)$$

Subscripts dr and df correspond to the direct and diffuse components of the radiance, respectively. If the atmospheric optical depth τ_{atm} is known or can be calculated, the direct component of the downward radiance $I_{\lambda,dr}^{\downarrow}(\tau, \mu)$ at snow optical depth τ can be measured or obtained as

$$I_{\lambda,dr}^{\downarrow}(\tau, \mu) = \frac{1}{2\pi} F_{\lambda}^S e^{-(\tau+\tau_{atm})/\mu_0} \delta(\mu - \mu_0), \quad (4)$$

where F_{λ}^S is the spectral irradiance at the top of the atmosphere and μ_0 is the cosine of the solar zenith angle. The present model can be applied to a coupled atmosphere-snow system if the atmospheric conditions are known.

[8] The total extinction coefficient σ_{ext} and the absorption coefficient σ_{abs} depend on the number concentration of particles n (total particles divided by total volume) and their absorption cross section C_{abs} and scattering cross section C_{sca} [Bohren and Barkstrom, 1974]:

$$\begin{aligned} \sigma_{ext} &= nC_{ext}, \quad \sigma_{sca} = nC_{sca}, \quad \sigma_{abs} = nC_{abs}, \quad C_{ext} = C_{sca} + C_{abs}, \end{aligned} \quad (5)$$

where C_{ext} is the extinction cross section. $\omega_0 \equiv \sigma_{sca}/\sigma_{ext} = \sigma_{sca}/(\sigma_{abs} + \sigma_{sca})$ is the single-scattering albedo. For simplicity, the snow grains are treated as spheres. Because only albedo rather than the bidirectional reflectance distribution function (BRDF) is considered, the effect of nonsphericity of snow grains is thus neglected. Errors resulting from this assumption should be smaller for metamorphosed or old snow than new snow. For a spherical scatterer, the grain size parameter is defined as $x = 2\pi a/\lambda$, where a is the radius of the spherical particle, and λ is the wavelength of the incident radiation. The single-scattering and absorption properties are computed using a combination of a Mie code Mie0 [Wiscombe, 1980] for $x \leq 300$, and a geometrical optics code GOMsphere [Zhou et al., 2003] for $x > 300$ as the results from both codes agrees well with difference in absorption efficiency $<4\%$ for $x > 300$. Mie0 is good for small size parameters and GOMsphere code is good for absorptive dielectric spheres of large size parameters. One advantage of GOMsphere is that there is no upper limit for size parameter and there is no ripple structure. The optical properties calculated using these codes are input into equation (1) so that the azimuthally averaged radiance at any zenith angle can be computed.

[9] In the following sections, the main task is to solve equation (1) for $I_{\lambda,df}^{\downarrow}(\tau, \mu)$ and $I_{\lambda,df}^{\uparrow}(\tau, \mu)$ using the discrete ordinate method radiative transfer (DISORT) algorithm [Stamnes et al., 1988]. Then, substituting these with equation (4) into equation (3), we obtain the upward and downward radiances at any optical thickness level and any viewing zenith angle. The monochromatic upward and downward fluxes or spectral irradiances are

$$F_{\lambda}^{\uparrow}(\tau, \mu_0) = 2\pi \int_0^1 d\mu \mu I_{\lambda}^{\uparrow}(\tau, \mu_0, +\mu) = 2\pi \int_0^1 d\mu \mu I_{\lambda}^{\uparrow}(\tau, \mu_0, \mu) \quad (6)$$

$$F_{\lambda}^{\downarrow}(\tau, \mu_0) = 2\pi \int_0^1 d\mu \mu I_{\lambda}^{\downarrow}(\tau, \mu_0, -\mu) = 2\pi \int_0^1 d\mu \mu I_{\lambda}^{\downarrow}(\tau, \mu_0, \mu). \quad (7)$$

The spectral albedo by definition is

$$\alpha_{\lambda}(\tau, \mu_0) = \frac{F_{\lambda}^{\uparrow}(\tau, \mu_0)}{F_{\lambda}^{\downarrow}(\tau, \mu_0)}. \quad (8)$$

[10] The optical depth for each homogeneous layer within the snowpack is

$$d\tau^i = \sigma_{\text{ext}}^i dz^i = \frac{3Q_{\text{ext}}^i \rho_{\text{snow}}^i dz^i}{4a^i \rho_{\text{ice}}}, \quad (9)$$

where a^i , ρ_{snow}^i and dz^i are the snow grain radius, the snow mass density (kg m^{-3}) and the thickness of the i th layer. Q_{ext}^i is the corresponding extinction efficiency. $\rho_{\text{ice}} = 917 \text{ kg m}^{-3}$ is the density of pure ice. $\rho_{\text{snow}}^i dz^i$ is the snow water equivalence. As the semi-infinite depth of snow for a specific wavelength is one key parameter investigated in this paper, we take the option that snow depth and density are treated separately, but it should be noted that the model depends on the depth-density product, rather than on either term independently. Equation (5), along with the number concentration of snow grains

$$n = \frac{\rho_{\text{snow}}}{\frac{4}{3}\pi a^3 \rho_{\text{ice}}}$$

and

$$C_{\text{ext}} = \pi a^2 Q_{\text{ext}},$$

have been used in obtaining equation (9).

3. Sensitivity Study I: Vertically Homogeneous Snow Cover

[11] Light transmitted into a snowpack will attenuate with snow depth. An optically semi-infinite depth is defined here as the snow depth beyond which an increase of snow depth does not have any effect on the snow reflectance, the subsequent albedo is called semi-infinite albedo. The minimum depth for a snow cover to be optically semi-infinite is called the critical snow depth (CSD). The numerical calculation of CSD is controlled as the depth h_{CSD} at which the difference between the albedo $\alpha_{\lambda}(h_{\text{CSD}})$ and $\alpha_{\lambda}(\infty)$ for an optically infinite snowpack is within 1% [Wiscombe and Warren, 1980]. For convenience, CSD is also referred to as the semi-infinite depth, with the understanding that any depth beyond CSD (but not infinite) is a semi-infinite depth. The semi-infinite albedo referred to in this section is the albedo calculated from a snow pack of at least 2 m depth for each case studied.

[12] Suppose a vertically heterogeneous snowpack is so thick that it can be regarded as semi-infinite. The whole snow depth is subdivided into many virtual layers, depending on the iteration space step, which is mainly determined by the wavelength. Each virtual layer is called a computational layer. The computation of the CSD begins with the first computational layer, do the radiative transfer calculations, add an additional computational layer, repeat the calculation until the albedo of the multilayer snow pack

reaches 99% of the semi-infinite albedo of the snow pack, then the total depth is the CSD for the wavelength in question. The CSD is calculated by iteration with variable iteration space step, depending on wavelength due to the greater absorptivity of snow in the NIR relative to the visible. Calculation of the CSD for the NIR needs finer space steps in the iteration calculation.

3.1. Spectral Semi-infinite Depth of Snow: Vertically Homogeneous Snow Cover

[13] For a snowpack that is thicker than the CSD, the albedo for a specific wavelength will be approximately constant, independent of additional layers beyond this depth. The scattering and absorption properties of snow are wavelength-dependent; the depth required for a snow cover to be optically semi-infinite is thus also wavelength-dependent. To study the spectral CSD, we use the DISORT algorithm [Stamnes *et al.*, 1988] along with equation (9) to solve equations (1) and (8) so that the spectral albedo for any thickness of the snowpack is obtained. For the sensitivity study, the base of the snow cover is assumed to be a black surface with zero reflectivity for any wavelength. In modeling aimed at comparison with the measured spectral albedo of the snowpack on sea ice (compare section 5), we use the albedo of cold bare first-year sea ice [Perovich, 1996, Figure 7] if the snow-ice interface is not flooded, and the albedo of nilas if the base of the snowpack is slush [Allison *et al.*, 1993, Figure 9], because the spectral albedo for slush is not available. Because nilas generally is covered by a mixture of snow, ice, and liquid water, it should have an albedo similar to that of slush, which is just a little bit higher than that of water. If the slush on top of thick first-year sea ice is thin enough so that the light can penetrate, it is possible that the albedo of nilas may be a little bit lower than the real case. The effect of the base on the surface reflectance depends ultimately on the thickness of the overlying snowpack.

[14] Snow density is very variable. New snow has small grain size and low density. From Paterson [1994, Table 2.1], the density for new to wind packed snow ranges from 50–400 kg m^{-3} . Wind-packed polar snow near the surface generally has small grain size and relatively high density. Seasonal snow generally has a density below 550 kg m^{-3} . Thus we take 550 kg m^{-3} as the upper limit of snow density for our sensitivity study below. We also take 100 kg m^{-3} as an example of fresh snow density and 330 kg m^{-3} as a typical density value for windpacked snow in the following discussion.

[15] Figure 2 shows the CSDs required for a snowpack to become semi-infinite versus wavelength for different combinations of grain size and density when the incident light is a direct beam with incident zenith angle $\theta_0 = 60^\circ$. Figures 2a and 2b are for snowpacks of low density (100 kg m^{-3}). Figure 2a is an example of a fresh (or new) snow pack, while Figure 2b is more of hypothetical sense to examine the impact of grain size on the penetration depth. Figures 2c and 2d are for snowpacks of intermediate snow density (330 kg m^{-3}). Figure 2c is an example of windpacked snow. Figures 2e and 2f are for well metamorphosed old snowpacks with coarse to very coarse grain size and high density (composite grains or depth hoar). For a fine-grained and low-density snow pack, the maximum critical depth (about

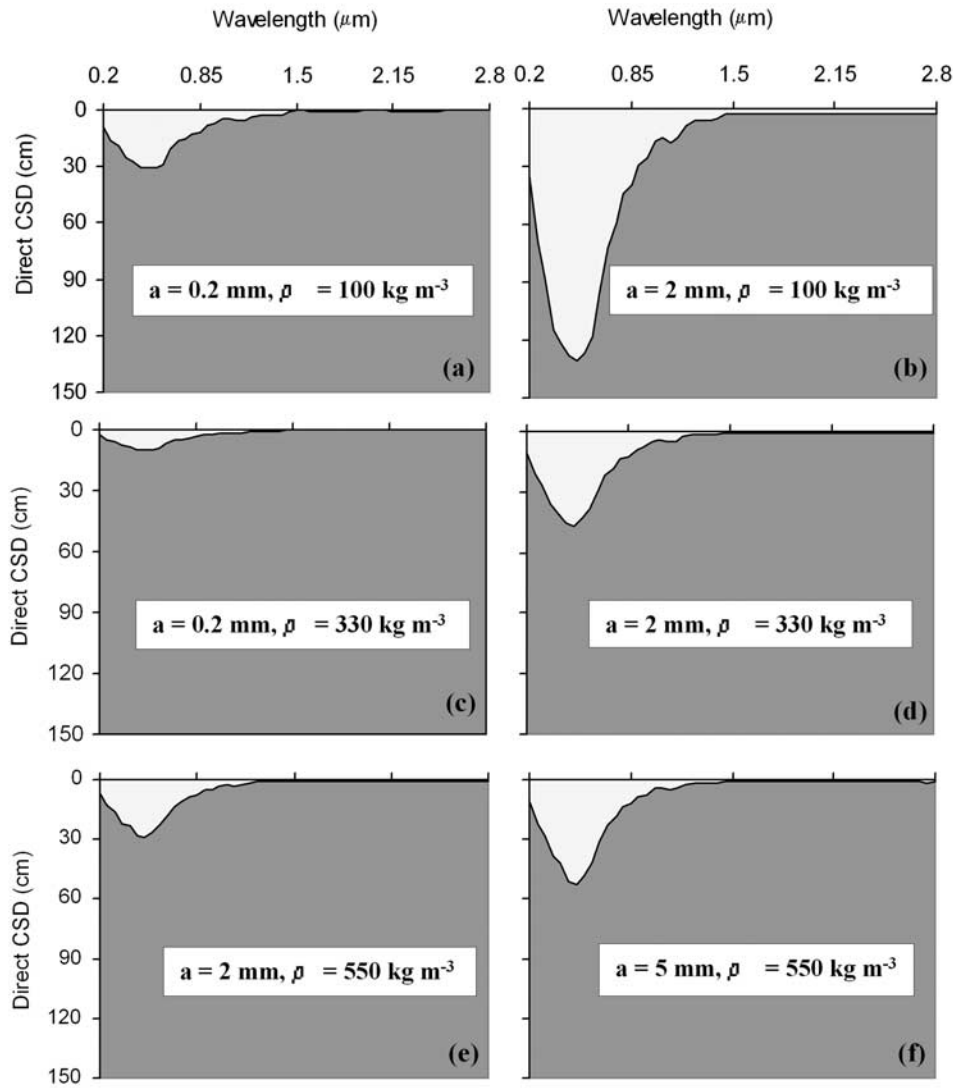


Figure 2. Spectral critical snow depth (CSD) for direct-beam incident radiation. The snow cover is treated as semi-infinite when the snow depth exceeds the critical depth. The solar zenith angle $\theta_0 = 60^\circ$. (a) Snow grain radius $a = 0.2$ mm, density $\rho = 100$ kg m $^{-3}$; (b) snow grain radius $a = 2$ mm, density $\rho = 100$ kg m $^{-3}$; (c) snow grain radius $a = 0.2$ mm, density $\rho = 330$ kg m $^{-3}$; (d) snow grain radius $a = 2$ mm, density $\rho = 330$ kg m $^{-3}$; (e) snow grain radius $a = 2$ mm, density $\rho = 550$ kg m $^{-3}$; and (f) snow grain radius $a = 5$ mm, density $\rho = 550$ kg m $^{-3}$. See color version of this figure in the HTML.

30 cm) occurs at wavelength around $0.5 \mu\text{m}$ (Figure 2a). Figure 2b is for a snowpack whose grain radius is 10 times larger ($a = 2$ mm) but the density is the same as Figure 2a. We can see that increase of the grain size enhances the penetration depth at all wavelengths from comparisons of Figures 2a and 2b, Figures 2c and 2d, and Figures 2e and 2f. The effect of snow densification on the semi-infinite depth can be seen by comparison between Figure 2a and Figure 2c, or among Figure 2b, Figure 2d, and Figure 2e.

[16] For a snowpack of low density ($\rho = 100$ kg m $^{-3}$) and medium density ($\rho = 330$ kg m $^{-3}$), an increase of the grain radius from 0.2 mm to 2 mm (ratio = $1/10$), yields an increase in the maximum semi-infinite depth at $\lambda = 0.5 \mu\text{m}$ from about 31 cm to about 130 cm (ratio = $1/4.2$) (Figure 2a compared to Figure 2b) for low-density case, and from about 10 cm to about 47 cm (ratio = $1/4.7$) (Figure 2c

compared to Figure 2d) for the intermediate density case. For high-density old snow ($\rho = 550$ kg m $^{-3}$), however, when the grain radius increases from 2 mm to 5 mm (ratio = $1/2.5$) (Figure 2e compared to Figure 2f), the maximum semi-infinite depth at $\lambda = 0.5 \mu\text{m}$ increases from about 29 cm to about 52.5 cm (ratio = $1/1.8$). This may indicate that the higher the density, the larger the impact of the increase of grain size on the semi-infinite depth. Enlargement of the grain size increases the critical depth, but mainly in the visible region. For NIR wavelengths $>1.0 \mu\text{m}$, a snow thickness of 5 cm is sufficient to yield a semi-infinite optical depth (except for the hypothetical case Figure 2b), while for all cases examined, a snow depth of 3 cm is sufficient for a snowpack to be semi-infinite for NIR wavelength $>1.5 \mu\text{m}$. An increase of snow density for a fixed grain size (Figure 2a and Figure 2c, or Figure 2b, Figure 2d and Figure 2e) will decrease the

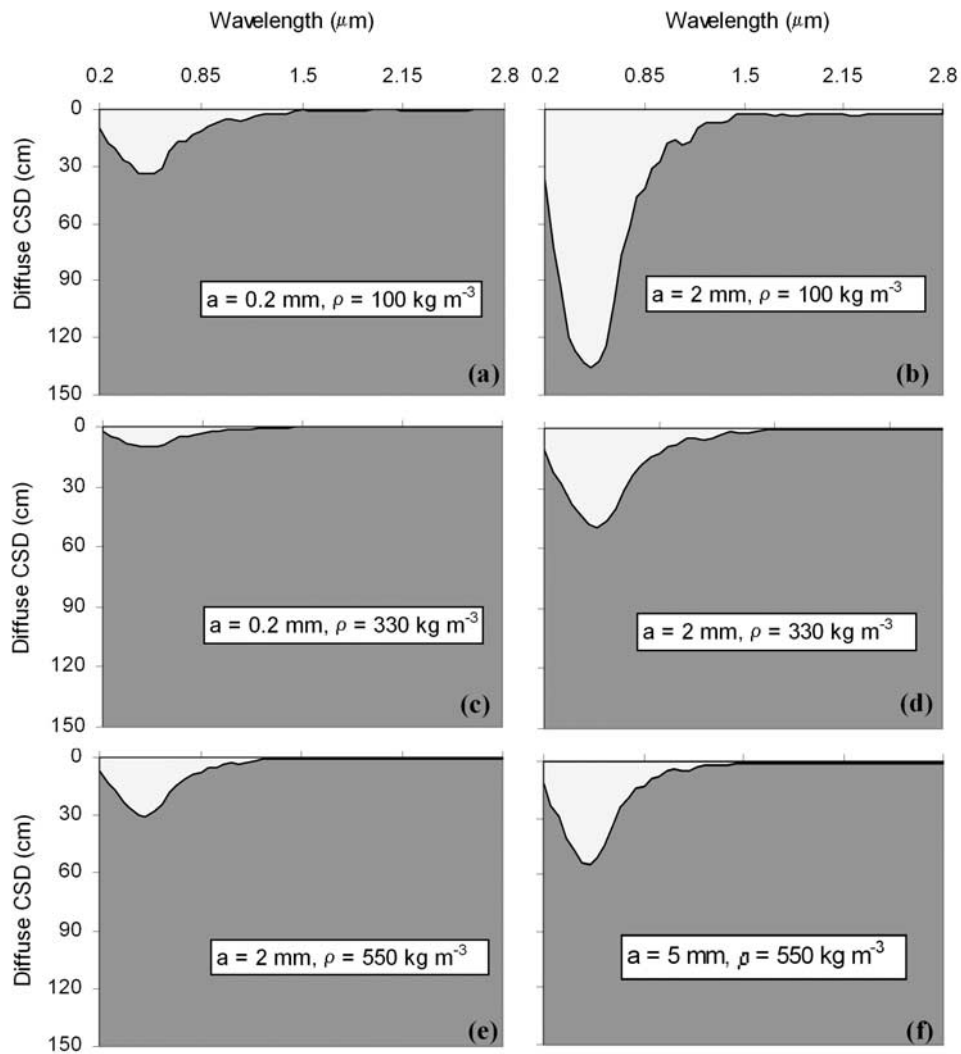


Figure 3. Same as Figure 2 but for diffuse incident radiation. See color version of this figure in the HTML.

critical depth, because it will increase the optical depth (see equation (9)) for the same snow layer, and thus enhance the extinction of the light rays within the snow. The consequence is that the light penetrates a smaller distance into the snow cover.

[17] Figure 3 is the diffuse counterpart of Figure 2. The incident radiation is assumed to be uniformly diffuse. For the same snowpack, the difference between the direct beam case and the diffuse incidence case is small. This is because the solar incident angle (60°) is close to the effective zenith angle of the purely diffuse radiation (about 50°) [Wiscombe and Warren, 1980]. It is expected that if the direct beam solar angle is very large (for instance 80°), the diffuse spectral albedo will be slightly smaller than the direct beam, or vice versa [Wiscombe and Warren, 1980]. The effects of grain size and density on CSD seen in Figure 2 for the direct beam case can also be inferred from Figure 3 for the diffuse incidence case: increasing grain size enhances the CSD and increasing density decreases the CSD.

[18] Although the snow CSD in the visible is as large as 47 cm when the grain radius is 2 mm and $\rho = 330 \text{ kg m}^{-3}$,

the dependence of snow albedo on snow depth is not linear. To quantify the nonlinearity of the contribution of snow depth to albedo, we compare the depth required to achieve 90% of the semi-infinite albedo with that required to achieve 99% of the semi-infinite albedo in the following discussion. The results are shown in Figure 4. All parameters for Figure 4 are the same as Figure 2 except that the calculation for Figure 4 is controlled by 90% instead of 99% of the semi-infinite albedo as is done for Figure 2. Comparison with Figure 2 indicates that the depth required to achieve 90% of the semi-infinite albedo is much smaller than that required to achieve 99% of the snow semi-infinite albedo. For new snow with fine grain size (Figure 2a and Figure 4a), the CSD is about 31 cm, but only 6 cm is needed for light at all wavelengths to achieve at least 90% of the semi-infinite albedo. In fact, 6 cm of snow is already deep enough for all wavelengths beyond $\lambda = 1.0 \mu\text{m}$ to reach their semi-infinite albedo (Figure 2a). For the case of larger snow grain radius ($a = 2 \text{ mm}$) and medium density (330 kg m^{-3}), to achieve 99% of the semi-infinite albedo, a maximum depth of about 47 cm (Figure 2d) is required,

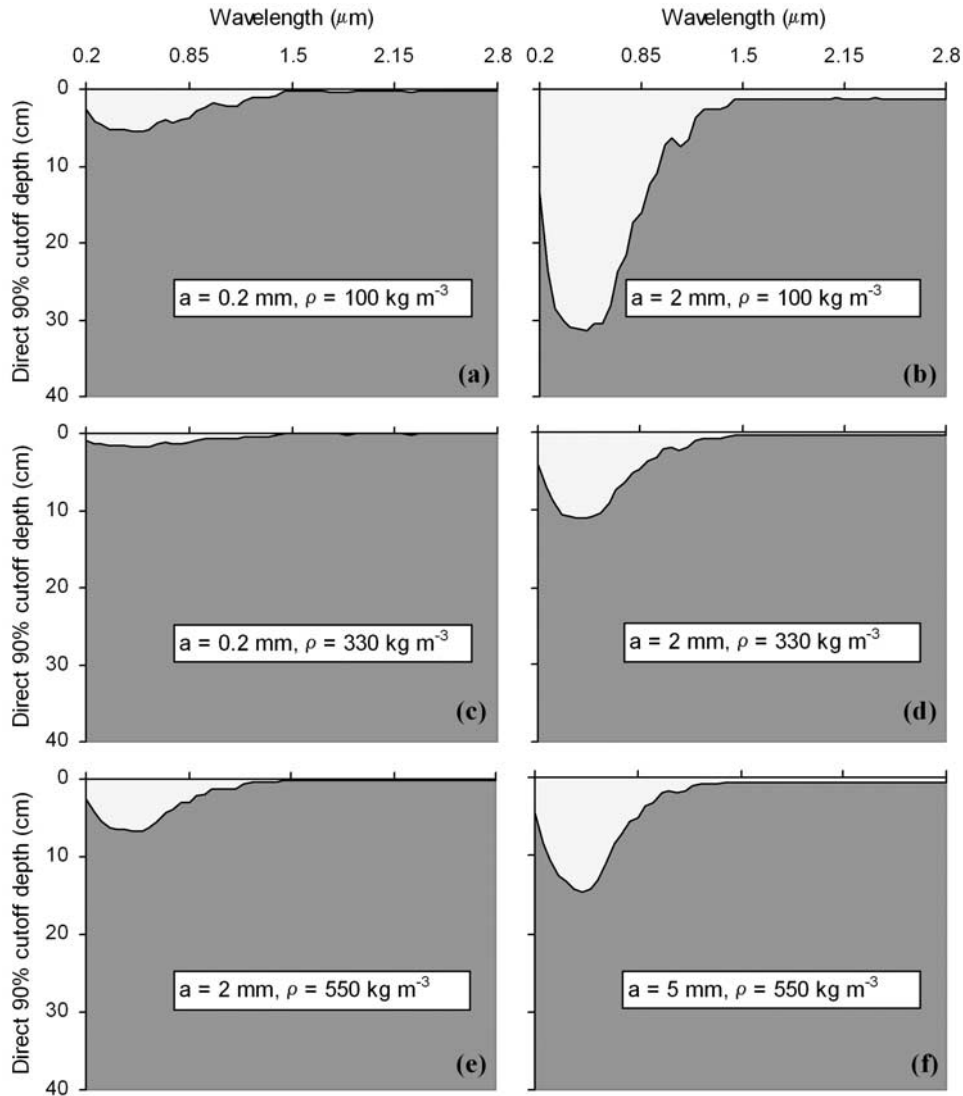


Figure 4. Spectral 90% cutoff depth of the semi-infinite albedo for direct-beam incident radiation. A 90% cutoff depth of the semi-infinite albedo is the snow depth required for the albedo to reach 90% of the semi-infinite albedo. Other parameters are the same as in Figure 2. See color version of this figure in the HTML.

while only about 11 cm is required (Figure 4b) for all wavelengths to achieve at least 90% of the semi-infinite albedo. In other words, out of 47 cm snow depth that contributes 99% of the semi-infinite albedo, the top 11 cm of snow contributes at least 90%, and the lower 36 cm contributes less than 9%. An 11 cm thick snow cover is semi-infinite for all wavelengths beyond $\lambda = 0.9 \mu\text{m}$ (Figure 2d). Consequently, it is expected that the top 11 cm of snow contributes significantly to the all-wave albedo for this case. For an old snowpack of large density (550 kg m^{-3}) and coarse grain size ($a = 2 \text{ mm}$), a depth of about 29 cm is required to achieve 99% of the semi-infinite albedo (Figure 2e), while only the top 7 cm is required to achieve at least 90% of the semi-infinite albedo (Figure 4e). The top 7 cm of snow is already semi-infinite for all wavelengths beyond $0.9 \mu\text{m}$ (Figure 2e).

[19] Compaction or densification will further decrease the depth required to achieve at least 90% of the semi-infinite albedo at $\lambda = 0.5 \mu\text{m}$ from 5.5 cm to 1.7 cm (Figures 4a

and 4c) for fine-grained snow pack, or from 35 cm through 11 cm to 6.7 cm (Figures 4b, 4d, and 4e) for coarse-grained snow pack. The decrease of the snow depth required to reach 90% of the semi-infinite albedo is even more significant for the case of very coarse composite (melt clusters, etc.) grain size ($a = 5 \text{ mm}$) and large density (550 kg m^{-3}) (Figures 2f and 4f). A depth of about 52.5 cm is required to achieve 99% of the semi-infinite albedo (Figure 2f), while only the top 15 cm is required to achieve at least 90% of the semi-infinite albedo (Figure 4f). This means that out of the 53 cm snow depth that contribute 99% of the semi-infinite albedo, the top 15 cm contribute 90%, while the lower 38 cm contributes the rest 9%. The top 15 cm of snow is already semi-infinite for all wavelengths beyond $0.8 \mu\text{m}$ (Figure 2f). A calculation was also carried out for a snowpack of grain radius $a = 1 \text{ mm}$ and a typical snow density $\rho = 300 \text{ kg m}^{-3}$: for wavelength $\lambda = 0.5 \mu\text{m}$, the CSD is about 21 cm, but the top 10 cm of snow contributes 97% and the top 3 cm

alone contributes 87%, which indicates the snow layer of 11 cm below a depth of 10 cm only contributes 2% to the albedo at the surface. A photon incident on the snow cover is most probably scattered back within the top 10 cm snow layer.

[20] Comparison of fine grain size cases with those of large grain size from Figures 2–4 shows that there is spectral detail in the near infrared for the $a = 0.2$ mm results that disappears for larger particles. This is because radiation in near infrared can be absorbed completely within one or two path lengths for large grain [Zhou *et al.*, 2003]. As is described at the beginning of section 3, the calculation of cutoff depth is obtained through iteration with a definite integral space (depth) step or resolution. For small grain size cases, if the spatial scale needed to resolve the spectral detail is smaller than the integral space step, the spectral difference cannot be resolved. To resolve the spectral features in the NIR, the iteration space step should be smaller than the grain size.

3.2. Depth of a Homogeneous Snow Cover “Probed” by MODIS Land Bands

[21] For visible and NIR (VNIR) sensors on a satellite, knowledge of the snow penetration depth for each VNIR channel is important for correct interpretation of retrieved snow parameters such as snow grain size and snow water equivalent retrieved from these sensors. As shown above, the CSD (also called 99% cutoff depth) and the cutoff depth of 90% of the semi-infinite albedo depend on wavelength. They also depend on the snow density and snow grain size. Figure 5 shows the snow cutoff depth versus the snow grain size for MODIS land bands for a snow cover with density $\rho = 400 \text{ kg m}^{-3}$. Here $a = 8$ mm is taken as the upper limit of snow grain size for this study. On the basis of the snow pit work on summer snow on sea ice, Morris and Jeffries [2001] found that composite grains account for 66%, with short dimension mainly in 2.5–3.0 mm, major dimension covering a broad range with a minor peak at 4.5–6.0 mm. Extreme large size can be >15 mm. The solar zenith angle is $\theta_0 = 60^\circ$. For visible bands (band 1 at $0.645 \mu\text{m}$, band 3 at $0.4656 \mu\text{m}$ and band 4 at $0.5536 \mu\text{m}$), the 99% cutoff depth varies from 5 cm for new snow ($a = 0.1$ mm) up to 75 cm for snow melt clusters ($a = 8$ mm). However, the 90% cutoff depth does not exceed 20 cm. For NIR band 2, the critical depth can be 20 cm, and the 90% cutoff depth is less than 7 cm. For the other three NIR bands, the critical depth is less than 3 cm. These results suggest that for the NIR channels of the MODIS land bands, the reflectance received is due to the very top 3 cm of snow, while for the visible channels, snow as deep as 75 cm may contribute to the reflectance for very old snow with a grain radius as large as 8 mm, although the top 20 cm of the snowpack is most important. For smaller grain sizes, the corresponding cutoff depth is reduced. Strictly speaking, the above comparison is a theoretical comparison. For a real comparison, the radiance data at a MODIS pixel needs to be converted to bidirectional reflectance and then to spectral albedo so that a comparison can be made. For a non-Lambertian surface, conversion from bidirectional reflectance to albedo is very difficult, unless the BRDF of the surface is known. Although efforts in both modeling and measurement of BRDF are going on [e.g., Leroux *et al.*, 1998, 1999], there

is not yet an operational algorithm for the conversion from bidirectional reflectance to spectral albedo [Stroeve and Nolin, 2002]. Within a MODIS pixel with resolution between 250 m to 1 km, the retrieved snow grain size based on the radiance of the pixel can only be interpreted as the optical mean snow grain size, though the snow pack of the pixel could be very inhomogeneous.

3.3. Depth of a Homogeneous Snow Cover “Probed” by a Sensor Aimed at Snow Grain Size Retrieval

[22] For snow grain size retrieval, Nolin and Dozier [2000] successfully used a set of spectral bands to obtain the effective optical snow grain size. This grain size should be the average value over the CSD layer. Figure 6 shows the CSD for various combinations of snow grain size and density for a spectral band centered at $1.03 \mu\text{m}$. The top curve is for a density of 100 kg m^{-3} , which represents a new snow cover. The bottom curve is for a snow density of 550 kg m^{-3} , which represents the upper limit of seasonal snow. This plot should cover the variations of density and grain size of a natural snow cover. As snow of small grain size is generally associated with smaller density, grain size retrieved from this band should lie in the lower part of the plot. For old snow with snow density generally larger than 300 kg m^{-3} , the CSD is not very sensitive to the snow grain size and density. For all cases that have snow density larger than 300 kg m^{-3} and snow grain radius between 0 to 2.5 mm, the retrieved grain size will represent a top snow layer of less than 5.2 cm. The snow parameter range within which the penetration depth for wavelength $\lambda = 1.03 \mu\text{m}$ is below 5 cm is shown as the whole area below the solid dotted line parallel to the snow grain radius axis. For most natural snow cover, 5 cm depth should be semi-infinite for $1.03 \mu\text{m}$ band.

4. Sensitivity Study II: Vertically Heterogeneous Snow Cover

[23] Owing to the vertical stratigraphic sequence, both the snow grain size and density increase from the top to the base of the snow pack. The snow grain radius was observed to increase from about 0.2 mm for new snow at the top of the snow to about 2 mm at a depth of 25 cm scale for snow cover on sea ice in winter [Sturm *et al.*, 1998]. On land, the average snow grain size and density show a remarkable variation from the top layers to the bottom layers [Grenfell *et al.*, 1994; Aoki *et al.*, 2000]. For instance, the range of half length of the major axis/minor axis of ice crystals can vary from (0.1–0.75 mm)/(0.05–0.1 mm) at the top to (0.25–1.0 mm)/(0.075–0.2 mm) at a depth of 10 cm, and the density varies between 120 kg m^{-3} at the top to 330 kg m^{-3} at a depth of 10 cm [cf. Aoki *et al.*, 2000, Figure 2a]. The variation of grain size within 1 cm vertical scale was also observed on the top of the snow on sea ice. For example, a depth of 1 cm new snow (grain radius ~ 0.2 mm) was frequently observed on medium-grained snow (grain radius ~ 1 mm) due to the frequent snow flurries [Zhou *et al.*, 2001]. This scale of vertical variability of snow grain size and density is within the semi-infinite depth of snow, and thus the vertical heterogeneity is expected to impact the reflectivity of snow. If the top layer of snow is homogeneous and thick enough ($>$ CSD), then the

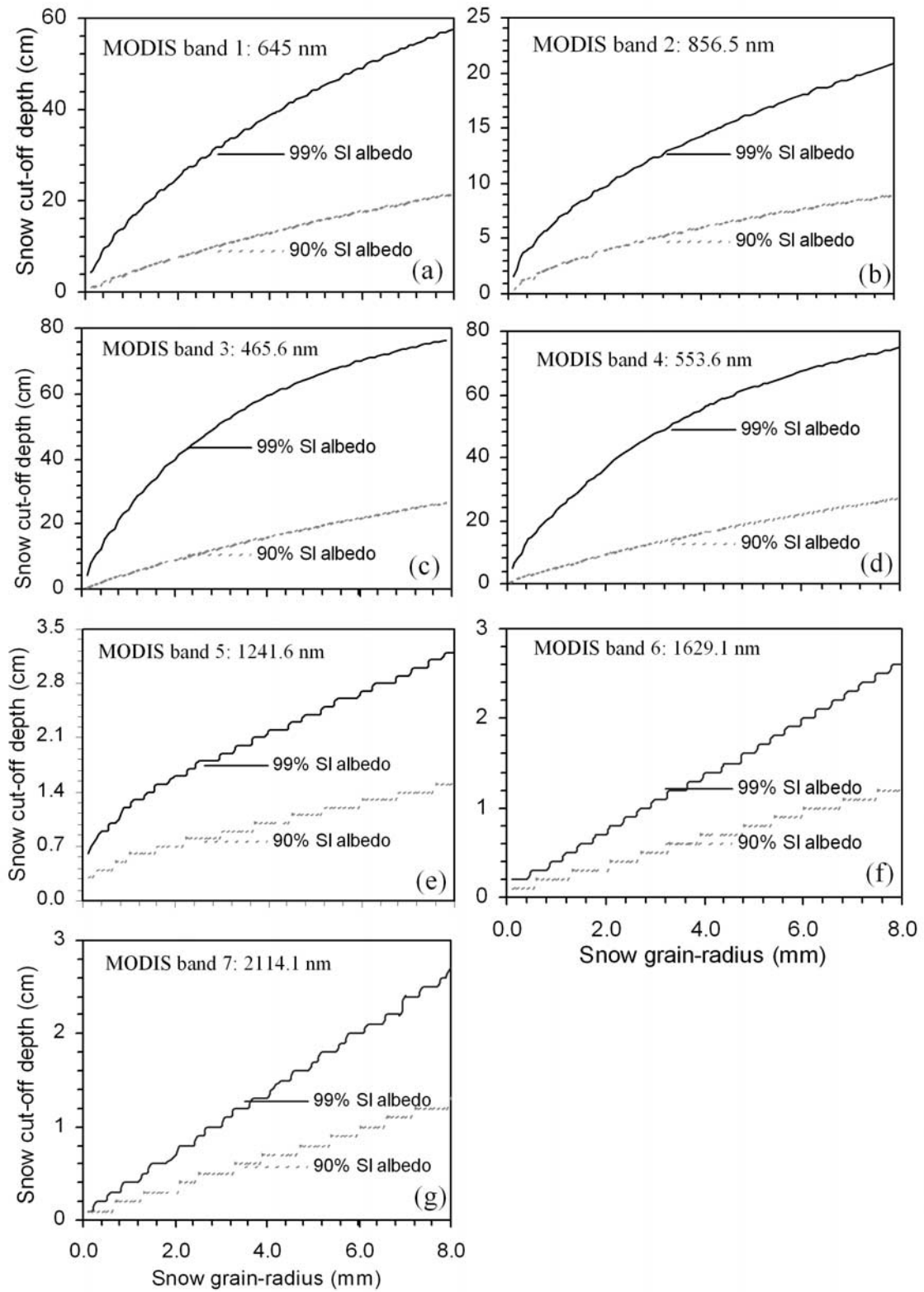


Figure 5. CSD and 90% cutoff depth of the semi-infinite albedo versus snow grain radius for MODIS land bands for direct-beam incident radiation: (a) band 1, (b) band 2, (c) band 3, (d) band 4, (e) band 5, (f) band 6, and (g) band 7. The solar zenith angle $\theta_0 = 60^\circ$. Snow density $\rho = 400 \text{ kg m}^{-3}$. SI, semi-infinite. See color version of this figure in the HTML.

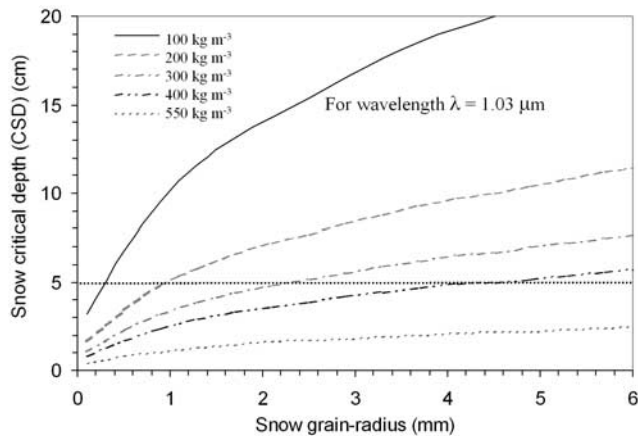


Figure 6. CSD of grain radius retrieving band $\lambda = 1.03 \mu\text{m}$ [Nolin and Dozier, 2000] for ranges of natural snow density and grain radius. For snow of a specific density the retrieved snow grain radius represents an average grain radius within the snow critical depth. See color version of this figure in the HTML.

multilayer model discussed below will automatically degenerate to the homogeneous one-layer model.

4.1. Effect of Vertically Inhomogeneous Grain Size on Spectral Semi-Infinite Albedo

[24] To separate the effect of grain size on albedo from other factors such as density and thickness, we simplify a snowpack as a snow cover having vertically constant density but vertically stratified grain size. The whole snow cover is assumed to be optically semi-infinite for all wavelengths and is subdivided into layers having different grain sizes. Each sublayer is treated as a homogeneous layer. Figure 7 shows the effect of different stratifications of grain size on the semi-infinite spectral albedo in the visible and NIR. The snow cover is assumed to be 1 m thick with a constant density ($\rho = 300 \text{ kg m}^{-3}$) from the snow surface to the bottom, with the top 6 cm being stratified and the bottom 94 cm being a homogeneous layer of grain radius $a = 1 \text{ mm}$. The top 6 cm is assumed to be stratified with six homogeneous layers, each 1 cm thick and having different snow grain sizes. Two cases of stratification are studied. Stratification case A (Figure 7a) is for a snowpack with grain radius increasing from 0.1 mm at the top to 5 mm at 6 cm, i.e., the gradient of snow grain size with respect to the depth from the surface is positive. This case represents the ideal case of a natural snow cover, for which aging and metamorphism result in increasing grain size with depth. However, for a real snowpack, intermittent snowfalls and warm weather may make the snow cover interweaved with layers of various grain sizes.

[25] Stratification case B is for a snowpack that has the reverse profile of case A for the top 6 cm, i.e., the grain size decreases with depth. Snow grain size is constant from 7 cm to the bottom (1 m) for both cases. The vertical grain size profiles for these two cases are shown in Figures 7a and 7b. The whole snow cover is optically semi-infinite. Figure 7c is for the diffuse spectral albedo of the two cases, while Figure 7d is for the direct beam (solar zenith angle

$\theta_0 = 56^\circ$). The CSDs for the two stratification cases are also calculated and shown in Figures 7e and 7f. Figure 7e is for diffuse incidence and Figure 7f is for the direct beam. For Figures 7c–7f, the solid curve is for stratification case A, and the dashed curve is for stratification case B. The albedo difference due to the two stratification cases is negligible for light within 0.3–0.6 μm spectral range. For wavelengths longer than 0.6 μm , the difference increases with wavelength. The longer the wavelength, the smaller the spectral albedo for stratification case B compared with case A.

[26] Although the average grain size is the same for the top 6 cm for the two stratification cases, different vertical distributions of grain size result in quite different spectral albedos. A comparison of Figure 7e with Figure 7f shows that the CSDs for stratification case A and B are very close between 0.3 and 0.8 μm and larger than 6 cm, the spatial scale of inhomogeneity of the snowpack. For wavelengths longer than 0.8 μm , the difference is obvious. Beyond 0.85 μm , the CSD for case A is smaller than 3 cm while for case B it is between 4 and 6 cm. If we attempt to retrieve the snow grain size using the 1.03 μm band that can reach up to 6 cm depth, it is expected that the retrieved grain size will be quite different for the two cases if the grain size profile is not taken into account, while the actual mean grain size and water equivalent are the same for both cases. The CSDs for both case A and case B at 1.03 μm do not exceed 6 cm. The grain size retrieved from case A is only from the top 2 cm (see Figures 7e–7f for case A), while from case B it is from the top 5 cm; thus the retrieved grain size for case A is apparently much smaller than that retrieved for case B. Grain size retrieved from NIR channels represents a homogeneous snow layer of very shallow depth. The smaller the grain size at the top of the real snowpack, the thinner the representative homogeneous snow layer. This indicates that NIR radiation is not only more sensitive than visible light to grain size but also more sensitive to the grain size in the top layers, resulting in a bifurcation of the spectral albedo for cases A and case B when the wavelength increases (Figures 7c and 7d). Here in Figure 7, along with Figure 8 (section 4.2), the wavelength axes is drawn from 300 to 1100 nm to keep the resolution in the spectral range as high as possible and in parallel with Figure 9 (section 5).

4.2. Effect of Vertically Inhomogeneous Snow Density on Spectral Semi-infinite Albedo

[27] The effect of the vertical inhomogeneity of the snow density is studied by adopting a snowpack with constant grain size, but with different densities from the top to the bottom of the snowpack. Figure 8 shows the effect of different stratifications of snow density on the semi-infinite spectral albedo in the VNIR region. As in Figure 7, the snowpack in Figure 8 is also assumed to have a total depth of 1 m, which is deep enough for the snow cover to be optically semi-infinite. The top 6 cm is stratified as follows: six homogeneous layers, each being 1 cm thick and having different densities. The grain radius is assumed to be $a = 0.5 \text{ mm}$. These cases are similar to those in Figure 7, with the grain size replaced by the density. Stratification case C and case D are shown in Figures 8a and 8b, respectively. In case C, the density increases from the top to 6 cm depth, and case D is the reverse of case C, i.e., the density

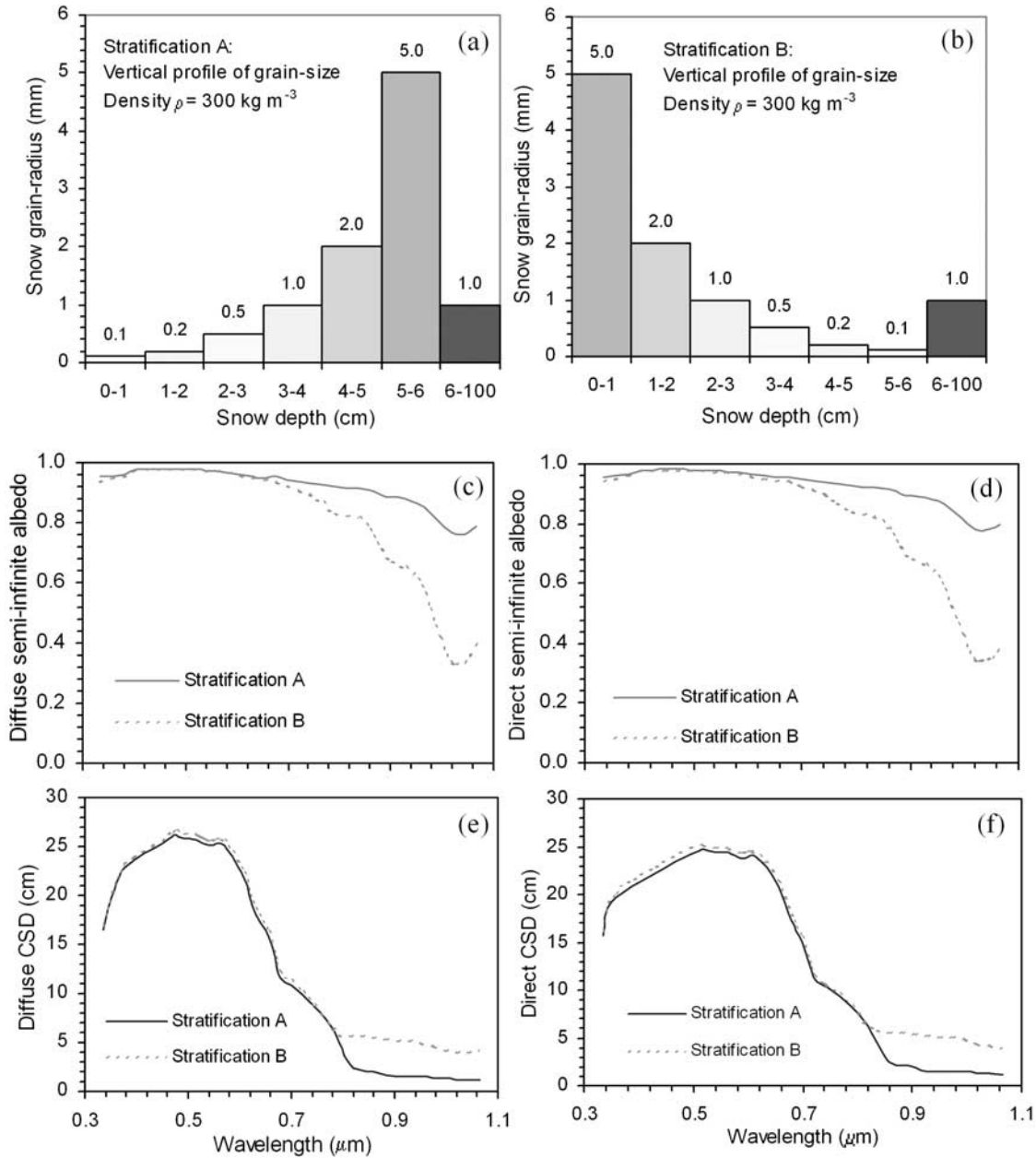


Figure 7. Effect of vertical profiles of snow grain radius on semi-infinite albedo and CSD for a snowpack of constant density ($\rho = 300 \text{ kg m}^{-3}$). (a) Vertical profile of grain radius for stratification A: The grain size increases with depth until 6 cm depth. (b) Vertical profile of grain size for stratification B: The grain radius decreases with depth until 6 cm depth. For both Figures 7a and 7b the number above each column is the grain radius in mm, and the grain size from 6 cm to 100 cm is constant. (c) Diffuse and (d) direct-beam spectral semi-infinite albedo for stratification case A and case B. (e) Diffuse and (f) direct-beam spectral CSDs for stratification case A and case B. See color version of this figure in the HTML.

decreases with the depth. Depth hoar layers within a snowpack are one of the few cases where the subsurface density is below that of the overlying layers.

[28] The spectral diffuse and direct beam semi-infinite albedos are shown in Figures 8c and 8d, respectively, for both case C and case D. From Figures 8c and 8d we can see that the vertical structure of density does not affect the semi-infinite spectral albedo, which is expected based on the results of *Wiscombe and Warren* [1980], *Bohren and*

Barkstrom [1974], and *Bohren and Beschta* [1979]. However, it will affect the spectral albedo if the snow depth is not semi-infinite for a particular wavelength, because the reflectivity of the base will contribute to the final results. The spectral diffuse and direct beam CSDs are shown in Figures 8e and 8f. The effect of the density structure can be seen in both Figures 8e and 8f. For wavelength $\lambda \leq 0.84 \mu\text{m}$, both density profiles result in almost the same CSDs. For wavelength $\lambda > 0.84 \mu\text{m}$, stratification case D

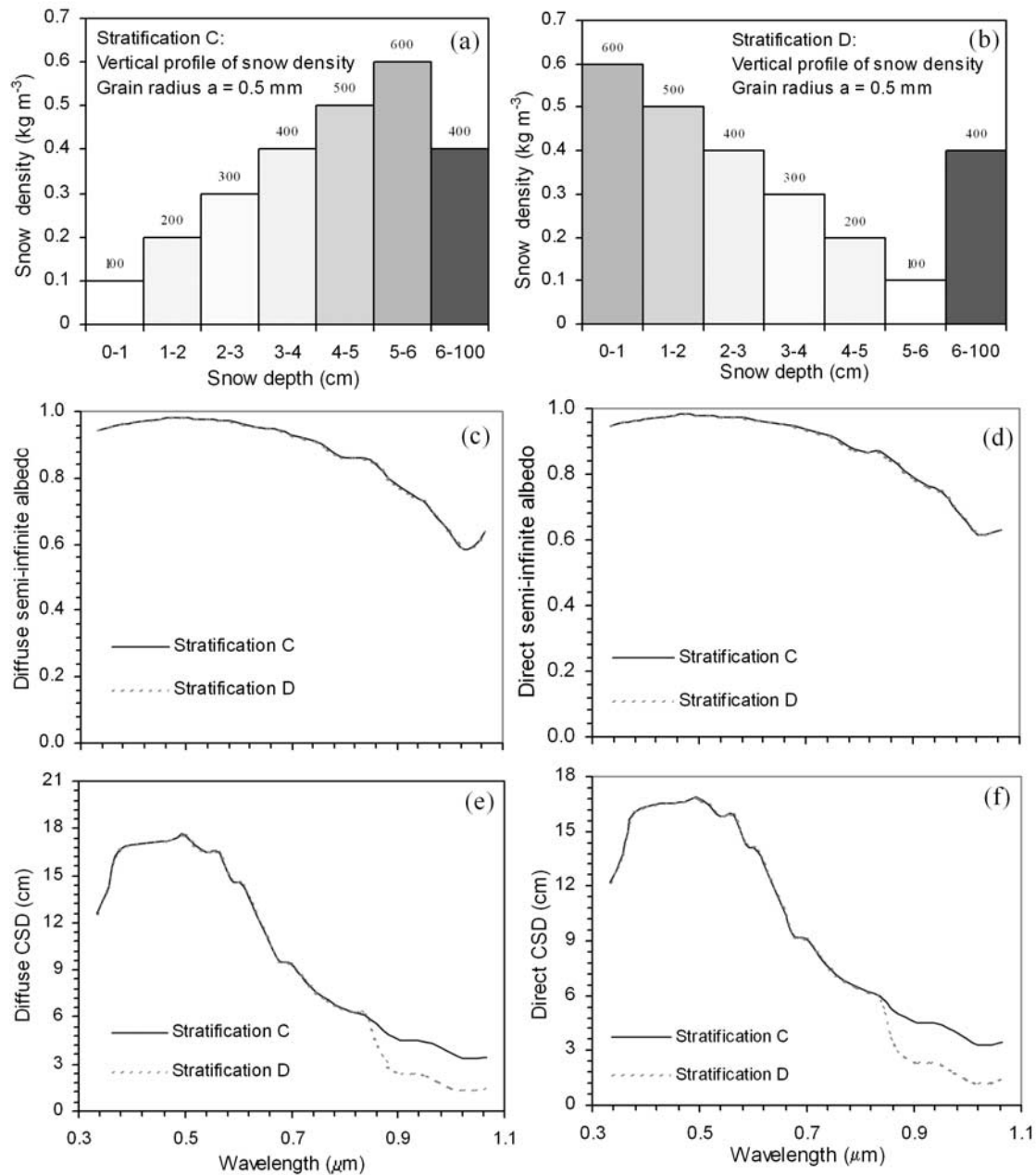


Figure 8. Effect of vertical profiles of snow density on semi-infinite albedo and CSD for a snowpack of constant grain radius ($a = 0.5$ mm). (a) Vertical profile of density for stratification C: The density increases with depth until 6 cm depth. (b) Vertical profile of density for stratification D: The density decreases with depth until 6 cm. For both Figures 8a and 8b the number above each column is the density in kg m^{-3} , and the density from 6 to 100 cm is constant. (c) Diffuse and (d) direct-beam spectral semi-infinite albedo for stratification case C and case D. (e) Diffuse and (f) direct-beam spectral CSDs for stratification case C and case D. See color version of this figure in the HTML.

results in a much smaller CSD than stratification case C because the increase of optical depth with geometrical depth is faster for case D, which has higher density at the top, than for case C, which has lower density at the top. When the penetration depth exceeds the spatial scale of the inhomogeneity of the top layer of snow (assuming it is homogeneous beyond this inhomogeneity scale), the density stratification within the inhomogeneity layer does not

matter as far as the spectral albedo is concerned. However, for a wavelength whose penetration depth is shallower than the inhomogeneity scale (for Figure 8, it is 6 cm), the density stratification does affect the penetration depth (grain size is assumed constant), though the spectral albedo is not affected because the snow is semi-infinite. For instance, the penetration depth of the 1.03 μm band is 3.3 cm (< 6 cm) for stratification C and 1.3 cm for

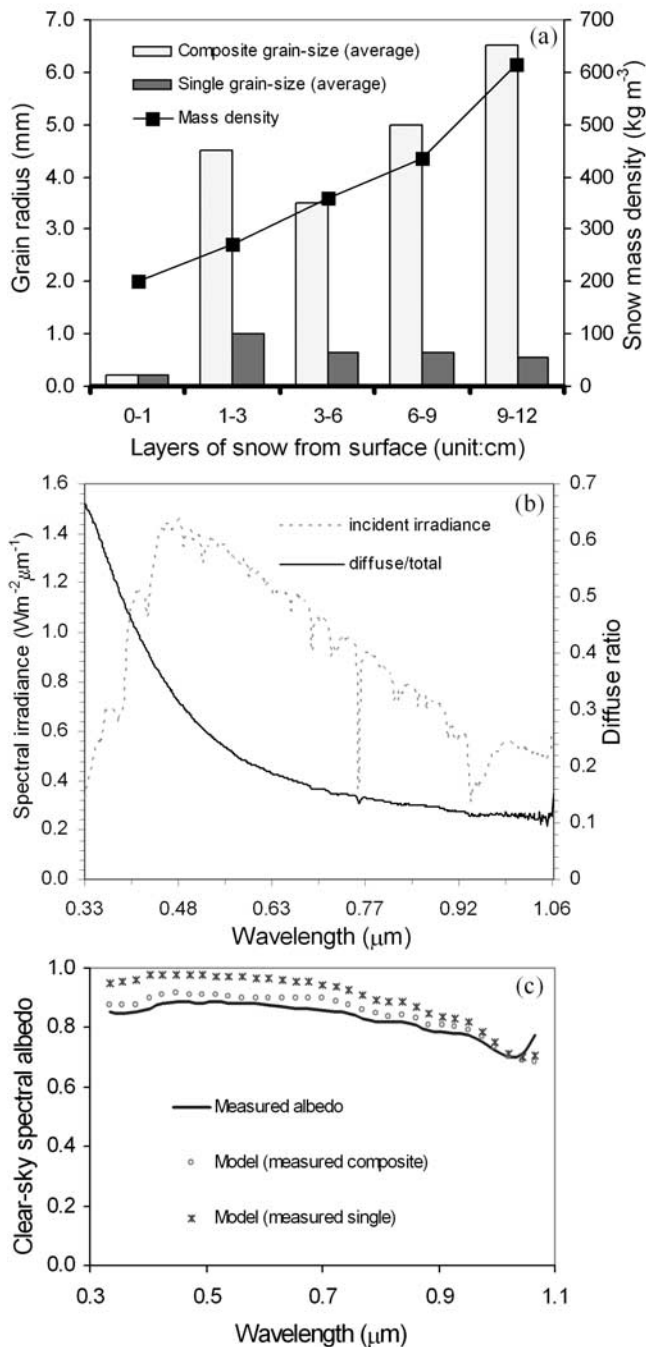


Figure 9. Comparison of modeled spectral albedo with measured spectral albedo. (a) Vertical profile of composite and single-grain radius and snow density. (b) Incident spectral irradiance and ratio of diffuse to total irradiance. Solar zenith angle $\theta_0 = 56^\circ$. (c) Measured spectral albedo and modeled results. See color version of this figure in the HTML.

stratification D. The remote sensing implication of the effect of density structure on the snow spectral albedo is that, if $\lambda = 1.03 \mu\text{m}$ is used to retrieve any snow parameter, the result will be representative of the top 3.3 cm of the snow cover in case C and only the top 1.3 cm of the snow cover in case D. Therefore owing to the effect of the density stratification on spectral albedo snow parameters retrieved from NIR channels will represent a deeper snow depth for

new snow than for wind packed snowpack, though the retrieved snow grain size for these cases will be the same.

5. Comparison of Modeled Spectral Albedo With Measurements

[29] Albedo measurements along with snow pit work were carried out during a summer cruise to the Ross Sea, Antarctica, in January and February 1999 aboard the US research vessel *Nathaniel B. Palmer* (NBP99-1 cruise). Most measurements of spectral albedo and bidirectional reflectance were carried out under cloudy conditions but with the solar disk visible [Zhou *et al.*, 2001]. For clear sky conditions, the direct beam was shaded using a light baffle so that the incident diffuse spectral irradiance was measured. Along with the total incident spectral irradiance, the direct portion can also be obtained. In the following discussion, we will focus on a comparison of modeling results with measurements under clear-sky conditions.

[30] The measurements under clear-sky conditions were taken on 8 January 1999 (ice station 5) of NBP99-1 cruise [cf. Zhou *et al.*, 2001, Figure 1]. Measurements and modeling results for the snow cover of ice station 5, of the NBP99-1 cruise are compared in Figure 9. The site had a snow depth of 12 cm, below which was slush. The measurements of snow grain size and density were done in 3 cm thick layers, but the grain size at the very top 5 to 10 mm was closely examined, because a large change in grain size even in the top 5 mm can significantly impact the pattern of spectral albedo of snow cover [Grenfell *et al.*, 1994]. Vertical profiles of the grain size for both composite grains and single grains that make up the composite grains, and density of the snowpack are shown in Figure 9a.

[31] The density of the top 1 cm of the snow was not measured and was estimated as the average of new snow (133 kg m^{-3}) and the measured density of the top 3 cm. The downwelling spectral irradiance and the ratio of the diffuse to the total irradiance are shown in Figure 9b. The data in Figures 9a and 9b are used as inputs to the multilayer (5 layer) radiative transfer model. The solar zenith angle was about 56° . Spectral albedo in the visible and near infrared (VNIR) was measured using a high-spectral-resolution spectroradiometer manufactured by Analytical Spectral Devices, Inc. (ASD). The spectral reflectance and spectral radiance between 333.65 nm and 1064.9 nm were measured by a 512 channel silicon photodiode array, each channel (an individual detector itself) is geometrically positioned to receive light within a 1.4 nm bandwidth. The measured and calculated spectral albedos are shown in Figure 9c. Two cases are modeled. One is for measured large composite grains, while the second case is for the measured single grains. The measurements from sensors between 1043.44 nm and 1064.90 nm are not very reliable because their irradiance measurements fluctuated considerably compared to sensors at other wavelengths due to the reduced sensitivity of the silicon photodiode sensors at wavelengths beyond about 1000 nm. As the spectroradiometer covers a wavelength range from 333.65 nm to 1064.90 nm, it may miss the spectral bands in the near-infrared region where snow optical properties are more sensitive to grain size of the top layers of snowpacks. Comparison of the two cases with the measurements shows

that the modeled albedo agrees fairly well with the measurement when the input snow grain size is taken as the measured composite grain size. The modeled result is on average 2.8% (maximum 4.7%) higher than the measurement. The modeled albedo is on average 9.1% (maximum 13.7%) higher than the measured one if the input grain size is taken as the measured single grain size. The discrepancy between the measurements and the modeling results is smaller with composite grain size than with single grain size. This corroborates the finding that the all-wave albedo is statistically more significantly correlated with the composite grain size rather than the single grain size which accounts for only a small portion of the snow cover on sea ice [Morris and Jeffries, 2001; Zhou, 2002]. A 12 cm depth is not thick enough for the snowpack to be semi-infinite in the visible region. Thus the bottom surface (slush in this case) plays some role in determining the spectral albedo in the visible. The effective average grain size (diameter) for the snowpack derived from the field measurements is 4.88 mm.

[32] From the above comparison of modeled spectral albedo values with measurements under clear conditions we note that, the modeled spectral albedo from the multilayer model agrees better with the measured result when the measured composite grain size is used than when the measured single grain size is used. For the composite grain size, modeled results agree fairly well with the measured ones, but are still generally higher than the measurements in the visible. The discrepancy may be due to biomass [Painter *et al.*, 2001], which is absorptive in the visible region and exists in the snowpack, especially at the snow-ice interface and in the slush. We did not consider this factor, mainly due to the lack of information required to quantify it.

6. Discussion and Conclusions

[33] This investigation examines the effect of thickness and vertical structure of homogeneous and inhomogeneous snowpacks on the spectral snow albedo and critical snow depth (CSD) by using a multilayer radiative transfer model. The computed spectral albedo versus snow thickness for a homogeneous snowpack with various values of naturally occurring snow grain sizes and density values indicates that the albedo approaches an asymptotic value for a very shallow snow depth (~ 3 cm) at NIR wavelengths, while in the visible, the albedo of a snowpack overlying a black surface increases very rapidly with thickness of the uppermost portion of the snow cover. A thickness of 5 cm is enough for the snowpack to become semi-infinite for NIR radiation. In the visible, the uppermost 10 cm of the snow cover is found to be the most important, even though the CSD may be much larger than 10 cm when the grain size is large and the density is small. For instance, at wavelength $\lambda = 0.5 \mu\text{m}$ for a snowpack with 1 mm grain size and 300 kg m^{-3} density, the CSD is about 21 cm, but the top 3 cm and 10 cm of the snow cover contribute about 87% and 97%, respectively, to the albedo of a snowpack of 100 cm thickness. In the visible region, the CSD is much larger than in the NIR. However, the contribution of the lower part of the snowpack is much smaller than if it were placed at the top. The contribution of the top 10 cm layer (or any value that is smaller than the CSD) of snow to the overall albedo of the snowpack depends on the grain size and density within the

layer: the smaller the grain size or the larger the density, the larger the contribution.

[34] For MODIS visible bands (bands 1, 3 and 4) (see Figure 5), the CSD varies from 5 cm for new snow ($a = 0.1$ mm) up to 75 cm for snow melt clusters ($a = 8$ mm). $a = 8$ mm is taken here as the upper limit for the size parameter. On the basis of the concurrent snow pit work of the 1999 summer cruise [Morris and Jeffries, 2001], composite grains account for 66%, with short dimension mainly in 2.5–3.0 mm, major dimension covering a broad range with a minor peak at 4.5–6.0 mm. Extreme large size can be >15 mm. However, the 90% cutoff depth does not exceed 20 cm. For MODIS NIR band 2 ($0.8565 \mu\text{m}$), the CSD may be 20 cm and the 90% cutoff depth less than 7 cm. For the other NIR land bands (band 5, 6 and 7) (see Figure 5), the CSD is smaller than 3 cm. These results suggest that for the NIR channels, the reflectance received by the MODIS sensors is due to the very top 3 cm of snow, while for the visible channels, snow as deep as 75 cm may contribute to the reflectance, although most of it is due to the top 20 cm for snow grain radius as large as 8 mm. For smaller grain sizes, the corresponding cutoff depth is reduced.

[35] While the NIR albedo of a natural snowpack is very sensitive to the physical parameters of the very top layers of the snow (≤ 5 cm), the visible albedo is sensitive to snow physical parameters of much deeper snow layers. Thus not only should the top layers be examined with high spatial resolution, the snow stratification should be also recorded and snow grain size and snow density should be measured within each snow stratum for the whole snowpack. Grain size retrieved from remote-sensing NIR channels represents the weighted average of a snow layer within a particular depth (CSD) with heavier weights associated with upper layers. The smaller the grain size at the top of the real snowpack, the thinner the contributing snow layer.

[36] Studies of the effect of the vertical inhomogeneity of the snow grain size on the spectral albedo show that although the average grain sizes may be the same for two snowpacks, different vertical distributions of grain size within the very top few centimeters can result in quite different spectral albedos, especially at longer wavelengths. This is because radiation at NIR wavelengths is not only more sensitive than visible light to grain size, but also more sensitive to the grain size in the upper layers of the snow. Visible light is sensitive to snow parameters within a much larger depth range than NIR. As expected, the vertical structure of the density does not affect the semi-infinite spectral albedo. However, it does affect the CSD. A snow profile that has smaller density at the top has a larger CSD, especially for longer wavelengths. The contribution of a top layer with specified depth (e.g., 10 cm) to the overall spectral reflectance of the whole snowpack depends on the grain size and density: the smaller the grain size or the larger the density, the larger the contribution.

[37] The simulated spectral albedo from a multilayer snow model agrees better with the measured results when the measured composite grain size rather than the measured single grain size is used. The composite grain size leads to modeled results that agree fairly well with the measured ones, but they are still 2.8% on average higher than the measurements in the visible. Biomass, ubiquitously ob-

served in the snowpack, especially at the snow-ice interface, may play an important role in reducing this gap.

[38] **Acknowledgments.** Snow pit work data for NBP99-1 cruise were measured and made available by Kim Morris (University of Alaska Fairbanks). Thanks go to the anonymous reviewers for the very helpful comments and suggestions. K. Stamnes acknowledges support from the National Space Agency of Japan (NASDA) and the US National Science Foundation. This work was supported by the National Aeronautics and Space Administration under grant NAG5-6338 to the University of Alaska Fairbanks (PI: Prof. Shusun Li).

References

- Allison, I., R. E. Brandt, and S. G. Warren, East Antarctic sea ice: Albedo, thickness distribution, and snow cover, *J. Geophys. Res.*, *98*, 12,417–12,429, 1993.
- Aoki, T., T. Aoki, M. Fukabori, A. Hachikubo, Y. Tachibana, and F. Nishio, Effects of snow physical parameters on spectral albedo and bidirectional reflectance of snow surface, *J. Geophys. Res.*, *105*, 10,219–10,236, 2000.
- Armstrong, R. L., A. Chang, A. Rango, and E. Josberger, Snow depths and grain-size relations with relevance for passive microwave studies, *Ann. Glaciol.*, *17*, 171–176, 1993.
- Bohren, C. F., and B. R. Barkstrom, Theory of the optical properties of snow, *J. Geophys. Res.*, *79*, 4527–4535, 1974.
- Bohren, C. F., and R. L. Beschta, Snowpack albedo and snow density, *Cold Reg. Sci. Technol.*, *1*, 47–50, 1979.
- Chang, A. T. C., J. L. Foster, D. K. Hall, A. Rango, and B. K. Hartline, Snow water equivalent determination by microwave radiometry, *Tech. Mem. 82074*, NASA Goddard Space Flight Cent., Greenbelt, Md., 1981.
- Colbeck, S. C., The layered character of snow covers, *Rev. Geophys.*, *29*, 81–96, 1991.
- Colbeck, S., E. Akitaya, R. Armstrong, H. Gubler, J. Lafeuille, K. Lied, D. McClung, and E. Morris, The international classification for seasonal snow on the ground, 23 pp., Int. Comm. on Snow and Ice of the Int. Assoc. of Sci. Hydrol., Gentbrugge, Belgium, 1990.
- Green, R. O., J. Dozier, D. Roberts, and T. Painter, Spectral snow-reflectance models for grain-size and liquid-water fraction in melting snow for the solar-reflected spectrum, *Ann. Glaciol.*, *34*, 71–73, 2002.
- Greenfell, T. C., and G. A. Maykut, The optical properties of ice and snow in the Arctic Basin, *J. Glaciol.*, *18*, 445–463, 1977.
- Greenfell, T. C., S. G. Warren, and P. C. Mullen, Reflection of solar radiation by the Antarctic snow surface at ultraviolet, visible, and near-infrared wavelengths, *J. Geophys. Res.*, *99*, 18,669–18,684, 1994.
- Jeffries, M. O., A. L. Veazey, K. Morris, and H. R. Krouse, Depositional environment of the snow cover on West Antarctic pack-ice floes, *Ann. Glaciol.*, *20*, 33–38, 1994.
- Jeffries, M. O., H. R. Krouse, B. Hurst-Cushing, and T. Maksym, Snow ice accretion and snow cover depletion on Antarctic first-year sea ice floes, *Ann. Glaciol.*, *33*, 51–60, 2001.
- Joseph, J. H., W. J. Wiscombe, and J. A. Weinman, The delta-Eddington approximation for radiative flux transfer, *J. Atmos. Sci.*, *33*, 2452–2459, 1976.
- Knap, W. H., C. H. Reijmer, and J. Oerlemans, Narrowband to broadband conversion of Landsat-TM glacier albedos, *Int. J. Remote Sens.*, *20*, 2091–2110, 1999.
- Kumai, M., Identification of nuclei and concentrations of chemical species in snow crystals sampled at the South Pole, *J. Atmos. Sci.*, *33*, 833–841, 1976.
- Leroux, C., J.-L. Deuzé, P. Goloub, C. Sergent, and M. Fily, Ground measurements of the polarized bidirectional reflectance of snow in the near-infrared spectral domain: Comparisons with model results, *J. Geophys. Res.*, *103*, 19,721–19,731, 1998.
- Leroux, C., J. Lenoble, G. Brogniez, J. W. Hovenier, and J. F. De Haas, A model for the bidirectional polarized reflectance of snow, *J. Quant. Spectrosc. Radiat. Transfer*, *61*, 273–285, 1999.
- Li, W., K. Stamnes, B. Chen, and X. Xiong, Snow grain size retrieved from near-infrared radiances at multiple wavelengths, *Geophys. Res. Lett.*, *28*, 1699–1702, 2001.
- Morris, K., and M. O. Jeffries, Seasonal contrasts in snow cover characteristics on Ross Sea ice floes, *Ann. Glaciol.*, *33*, 61–68, 2001.
- Murozumi, M., T. J. Chow, and C. Patterson, Chemical concentrations of pollutant lead aerosols, terrestrial dusts and sea salts in Greenland and Antarctic snow strata, *Geochim. Cosmochim. Acta*, *33*, 1247–1294, 1969.
- Nolin, A. W., and J. Dozier, A hyperspectral method for remotely sensing the grain size of snow, *Remote Sens. Environ.*, *74*, 207–216, 2000.
- Painter, T. H., B. Duval, W. H. Thomas, M. Mendez, S. Heintzelman, and J. Dozier, Detection and quantification of snow algae with an airborne imaging spectrometer, *Appl. Environ. Microbiol.*, *67*, 5267–5272, 2001.
- Painter, T. H., J. Dozier, D. A. Roberts, R. E. Davis, and R. O. Green, Retrieval of subpixel snow-covered area and grain size from imaging spectrometer data, *Remote Sens. Environ.*, *85*, 64–77, 2003.
- Paterson, W. S. B., *The Physics of Glaciers*, 3rd ed., Butterworth-Heinemann, Woburn, Mass., 1994.
- Perovich, D., The optical properties of sea ice, *Monogr. 96-1*, USA Cold Regions Res. and Eng. Lab., Hanover, N. H., 1996.
- Stamnes, K., S.-C. Tsay, W. Wiscombe, and K. Jayaweera, Numerically stable algorithm for discrete-ordinate-method radiative transfer in multiple scattering and emitting layered media, *Appl. Opt.*, *27*, 2502–2509, 1988.
- Stroeve, J. C., and A. W. Nolin, New methods to infer snow albedo from the MISR instrument with applications to the Greenland ice sheet, *IEEE Trans. Geosci. Remote Sens.*, *40*, 1616–1625, 2002.
- Sturm, M., K. Morris, and R. Massom, The winter snow cover of the West Antarctic pack ice: Its spatial and temporal variability, in *Antarctic Sea Ice: Physical Processes, Interactions and Variability*, *Antarct. Res. Ser.*, vol. 74, edited by M. O. Jeffries, pp. 1–18, AGU, Washington, D. C., 1998.
- Thomas, G. E., and K. Stamnes, *Radiative Transfer in the Atmosphere and Ocean*, Cambridge Univ. Press, New York, 1999.
- Warren, S. G., Optical properties of snow, *Rev. Geophys.*, *20*, 67–89, 1982.
- Warren, S. G., and A. D. Clarke, Soot in the atmosphere and snow surface of Antarctica, *J. Geophys. Res.*, *95*, 1811–1816, 1990.
- Wiscombe, W. J., Improved Mie scattering algorithms, *Appl. Opt.*, *19*, 1505–1509, 1980.
- Wiscombe, W. J., and S. G. Warren, A model for the spectral albedo of snow. I: Pure snow, *J. Atmos. Sci.*, *37*, 2712–2733, 1980.
- Zhou, X., Optical remote sensing of snow on sea ice: Ground measurements, satellite data analysis, and radiative transfer modeling, Ph.D. thesis, 219 pp., Univ. of Alaska, Fairbanks, 2002.
- Zhou, X., S. Li, and K. Morris, Measurement of all-wave and spectral albedo of snow surface on the summer sea ice in the Ross Sea, *Ann. Glaciol.*, *33*, 267–274, 2001.
- Zhou, X., S. Li, and K. Stamnes, Geometrical-optics code for computing the optical properties of large dielectric spheres, *Appl. Opt.*, *42*, 4295–4306, 2003.

S. Li, Geophysical Institute, University of Alaska Fairbanks, P. O. Box 757320, Fairbanks, AK 99775-7320, USA. (sli@asf.alaska.edu)

K. Stamnes, Department of Physics and Engineering Physics, Stevens Institute of Technology, Castle Point on Hudson, Hoboken, NJ 07030, USA. (kstamnes@stevens-tech.edu)

X. Zhou, Department of Earth and Environmental Science, New Mexico Institute of Mining and Technology, 801 Leroy Place, Socorro, NM 87801, USA. (xzhou@nmt.edu)